Solar Energy Materials & Solar Cells 216 (2020) 110701

Contents lists available at ScienceDirect

Solar Energy Materials and Solar Cells

journal homepage: http://www.elsevier.com/locate/solmat

Investigation on limiting factors affecting $Cu_2ZnGeSe_4$ efficiency: Effect of annealing conditions and surface treatment

Nada Benhaddou [a,b], Safae Aazou [a,b], Yudania Sánchez [c], Jacob Andrade-Arvizu [c], Ignacio Becerril-Romero [c], Maxim Guc [c], Sergio Giraldo [c], Victor Izquierdo-Roca [c], Edgardo Saucedo [c,d], Zouheir Sekkat [a,b,e,*]

[a] Department of Chemistry, Faculty of Sciences, Mohammed V University in Rabat, Morocco
[b] Optics & Photonics Center, Moroccan Foundation for Advanced Science, Innovation and Research – MAScIR, Rabat, Morocco
[c] Catalonia Institute for Energy Research -IREC, Sant Adrià de Besòs, Barcelona, Spain
[d] Photovoltaic Group, Electronic Engineering Department, Universitat Politècnica de Catalunya, C J. Girona 31, 08034, Barcelona, Spain
[e] Department of Applied Physics, Osaka University, 2-1 Yamadaoka, Suita, Osaka, Japan

ARTICLE INFO

Keywords:
CZGeSe
Kesterite solar cells
Selenization
Chemical etching
Photovoltaic

ABSTRACT

This work aims to unveil the optimal annealing conditions and surface treatments of CZGeSe absorbers, synthesized using vacuum-based deposition technique, with an eye to optimizing the main parameters allowing better control of secondary phases formation and improving crystalline quality of this absorber. Firstly, a comparative study is given of one and two-step annealing profiles, where, for each thermal treatment, the optimal temperature is probed. The second section of this study underlines the evaluation of the surface treatment effect on the as-annealed absorber using different etching agents. Finally, the effect of different post-annealing treatment temperatures on the overall performance of the fabricated devices is evaluated. For the studied optimizations, a deep understanding of the cell behavior is provided through structural, morphological and electrical characterizations. Preliminary results have given an efficiency up to 5.6% with higher V_{oc} = 572 mV and FF = 65% compared to the reported record cell using similar absorber (V_{oc} = 558 mV, FF = 59%). This performance is linked to the implementation of a two-step annealing process with lower temperatures (330 °C/480 °C) as it showed the best crystallinity-efficiency trade-off along with the smallest amount of ZnSe secondary phase among all the thermal routines studied. In addition, after the evaluation of several etching agents, the implementation of a KCN etching has shown to be the most effective leading to a remarkable improvement of the PN junction through a surface passivation.

1. Introduction

Throughout the different photovoltaic generations, especially in thin film PV technologies, the annealing step has been required to initiate the chemical reaction of elemental precursors, where the process conditions have been adequately optimized for each family of absorber materials. In the same vein, the photovoltaic community has recurrently demonstrated the paramount impact the thermal treatment has on different facets of the resulting absorber quality, including stoichiometry, grain size, surface morphology, defects in the absorber and its interfaces with Mo and CdS. Insufficient annealing temperature and/or time lead to unreacted elemental phases, thus showing altered stoichiometry and inappropriate material crystallinity. Chalcopyrite materials and especially in the case of CIS solar cells, it has been shown that poor morphological characteristics and porous surface using very short (~10 min) or very long (~90 min) reactive annealing time induce a significant impact on the device performance since conduction paths between the absorber and TCO were created through the pores [1]. As for Cu(In,Ga)$(S,Se)_2$ (CIGS/CIGSe) absorbers, a variation in the selenization stages appear to whether create detrimental effect on the adhesion to the substrate and peel-off issues (single annealing stage) or to strengthen the referential XRD diffraction peak indicating improved crystallinity of CIGS thin film (three sequential stages), whereas the annealing time above the optimal one may form detrimental secondary phases on the absorber surface. Furthermore, a shift in the diffraction peak position was witnessed at extended thermal treatments that could be resulting

* Corresponding author. Department of Chemistry, Faculty of Sciences, Mohammed V University, Rabat, Morocco.
E-mail addresses: s.aazou@mascir.ma, aazou@fsr.ac.ma (S. Aazou), z.sekkat@mascir.ma (Z. Sekkat).

https://doi.org/10.1016/j.solmat.2020.110701
Received 13 April 2020; Received in revised form 8 July 2020; Accepted 11 July 2020
Available online 6 August 2020

from the composition variations and/or residual stress in the films [2–5].

Polycrystalline CdTe photovoltaic absorber has confirmed the importance of the annealing conditions that monitor the grain growth and the grain boundaries, as they limit the V_{oc} and J_{sc} by forming recombination centers and trap states for charge carriers that reduce carrier mobility and lifetime [6]. On the other hand, it has been pointed out that small variations in annealing temperature could control the re-orientation structure of the thin film. More precisely, in the case of CdTe a structural transition from highly preferential (111) orientation to randomly oriented poly-crystals when heat-treated at 385 ± 5 °C was observed [7–9].

Although the absorber bulk composition is mainly controlled by optimized annealing conditions, a number of imperfections (Se vacancies, native oxides, secondary phases …) may still remain on its surface, being quite challenging to control their appearance. In this sense, surface pre-treatments of the absorber are revealed as a relevant step to improve the absorber morphology and ultimately boost the solar cells performance. Various selective etching agents were designed to fulfill the need of each technology. In CdTe for instance, many wet etching agents were used such as, HCl, Br_2–CH_3OH, $K_2Cr_2O_7$–H_2SO_4, CH_3NH_3I … to produce a Te-rich surface, this layer effectively leads to a p + doped layer inducing a reduction in the Schottky barrier at the back contact and higher photovoltaic parameters compared to the non treated absorbers [10,11].

The use of KCN etching agent in the case of CIGS has limited the excess of conductive ($Cu_{2-x}Se$) phase formed on the film surface, which represents a severe impediment against further enhancement in CIGS performance due to the shunt paths and the poor PN junction quality it creates [12,13]. Recently, NH_3 etching solution with proper concentration was used in the surface treatment of Cd free CIGS solar cells and succeeded to remove Se oxide, Na, In_2Se_3, Ga_2Se_3 from the CIGS film surface and to reduce the number of electronic defects in the junction, especially those affecting the barrier height at Zn(O,S)/CIGS interface. This has led to an improvement in all electrical parameters and an efficiency over 20% [14].

Kesterite $Cu_2ZnSn(S,Se)_4$ (CZTSSe) absorber material has emerged as a new alternative to CIGS and aims to overcome the shortcomings of this latter, especially, the indium scarcity and the toxicity of cadmium that limit the large scale production. This new compound presents the advantage of using low toxicity and earth-abundant elements. Additionally, this chalcogenide family is characterized by its high absorption coefficient and direct bandgap in the range of 1.0 eV–1.5 eV [15,16].

Kesterite solar cells seem to follow the same path as their counterparts, where thermal treatment and surface etching are indispensable steps in the synthesis. However, one of the difficulties facing this technology compared to its predecessor is the Sn loss at high temperature (i.e. T > 400 °C) that alters the stoichiometry of the quaternary phase [17]. Furthermore, The Sn related defects are recognized as the origin of persistent electron trapping/detrapping in kesterite photovoltaic devices, due to the multivalency of the Sn which creates donor defects generating deep recombination centers [18,19]. These defects have a direct impact on the V_{oc} deficit, which potentially degrades the device performance. In this sense, in order to reduce to some extent, the Sn-related drawbacks, researchers focused their studies and attention on the Ge incorporation into kesterite-based solar cells as a new promising way towards enhanced efficiencies. Finding the adequate synthesis conditions is a key factor to control the secondary phases formation (either at the interfaces or in the bulk), considered one major challenge facing the development of kesterite-based solar cells.

The pure Ge kesterite $Cu_2ZnGeSe_4$ has achieved an open circuit voltage of 744 mV as the highest V_{oc} up to date for this technology, which is close to the one of record CIGS solar cell (741 mV) [20]. This achievement encourages further investigations on this material. The substitution of Sn with Ge in the kesterite lattice leads to a proportional increase in the bandgap energy with the amount of Ge added. Theoretical calculations predict that this increase is due to the Ge capability to slightly upshift the conduction band minimum, whereas the valence band maximum remains at the similar initial level as $Cu_2ZnSnSe_4$ kesterite [21–23].

In this work, we provide a full comparative study of the effect of annealing profile, temperature and surface treatment and their interrelationship on the synthesis of pure Ge kesterite absorber quality. The synthesized CZGeSe kesterite is strongly influenced by slight changes in temperature and type of annealing profile. Thus, different annealing routines, including one-step and two-step, and different annealing temperatures will be evaluated. Additionally, as second optimization strategy, several chemical etchings/surface treatments, including commonly used KCN, $(NH_4)_2S$ or $KMnO_4$+ $(NH_4)_2S$ in acidic environment, will be tested on as-annealed absorbers and optimized, trying to understand what is/are the best possible surface treatment for this material. Finally, the impact of post-annealing treatments at different temperatures on full devices and their optoelectronic properties will be presented.

2. Materials and methods

2.1. Metallic stack deposition

CZGeSe is synthesized by the sequential deposition of Cu/Zn/Ge metallic precursors by means of DC magnetron sputtering (Alliance AC450) on Mo-coated SLG (soda-lime glass) substrates. The Mo layer is deposited by DC magnetron sputtering (750 nm, $R_{sheet} = 0.3\ \Omega/sq$). The identification of the compositional ratios of the as-deposited precursors and the CZGeSe absorber films is carried out using X-Ray Fluorescence (XRF, Fischer scope XVD), which is calibrated with inductively coupled plasma optical-emission spectroscopy (ICP-OES). The ratios of Cu/(Zn + Ge) and Zn/Ge are kept near 0.65 and 1.1, respectively. The total metallic stack thickness is around 540 nm.

2.2. Reactive annealing

The thermal treatment is performed in a conventional tubular furnace under Se environment. The selenization is carried out using a graphite box with elemental Se and $GeSe_2$ (100 mg and 5 mg, respectively). The annealing process adopts the same ramping rate 20 °C/min for both, one- and two-step annealing profiles. In the case of two-step thermal regime, the first step is performed at low pressure of 1.5 mbar whilst the second step is accomplished in 1 bar of inert gas atmosphere (Ar). The samples are cooled down naturally to room temperature.

2.3. Etching treatments

The surface treatment of these absorber layers is performed by 2 min dipping time using different etching agents: ammonium sulfide $(NH_4)_2S$, potassium cyanide KCN, and potassium permanganate followed by ammonium sulfide $KMnO_4$+$(NH_4)_2S$).

- $KMnO_4$ as oxidizer (0.01 M) in acidic environment (H_2SO_4) for 40 s followed by $(NH_4)_2S$ (22% v/v) for 2 min
- KCN (2% v/v)
- $(NH_4)_2S$ (22% v/v)

2.4. Device fabrication

CdS buffer layer is deposited onto the absorber layer by chemical bath deposition (CBD), followed by the deposition of the transparent conductive window layer (TCO) via DC-pulsed sputtering (Alliance AC100), which consists of sequential deposition of i-ZnO (50 nm) and ITO (200 nm). Thereafter, lateral isolation is done by means of micro-diamond scriber MR200 OEG to have 3 × 3 mm^2 cells. Neither anti-reflective coating nor metallic grids are used in the devices presented

in this work.

2.5. Characterization

J-V curves are measured by a calibrated 1-sun 3000 class AAA solar simulator (Abet Technologies, AM 1.5G illumination). The measurements are carried out at room temperature after calibration of the solar simulator with a c-Si reference cell.

Spectral response external quantum efficiency (EQE) measurements are made using a Bentham PVE300 system (Bentham Instruments Ltd, Berkshire, U.K.) calibrated with c-Si and Ge photodiodes.

Raman spectroscopy is performed using Horiba Jobin Yvon LabRam HR800-UV coupled with an Olympus metallographic used to distinguish the phases present in the resulting absorber.

SEM images are obtained with a ZEISS Series Auriga microscope using a 5 kV accelerating voltage.

3. Results and discussion

3.1. Effect of annealing profile and temperature

Undoubtedly, the annealing is a decisive step in the kesterite growth since it monitors the evolution of the absorber's morphology, crystallinity, and the intermediate phases formed during the thermal treatment. The impact on the growth mechanism and the resulting defects varies among literature with the annealing conditions (pressure, ramping rate, temperature, time, and so forth).

In the case of Sn-based kesterite, A. Fairbrother et al. [24] set the annealing temperature between 425 °C and 550 °C for 45 min under 1–2 mbar Ar flow, observing a significant increase of grain size with increasing the annealing temperature. However, this increment led to a morphology deterioration as well as the formation of voids at the Mo/CZTSe interface and deduced that a relatively low temperature of 450 °C is considered as an optimal working temperature. In another study, A. C. Lokhande and co-workers [25] investigated the effect of the annealing temperature among other annealing conditions, on Ge-doped CZTSSe. They observed that 550 °C is the optimal temperature compared to temperatures higher than 575 °C or lower than 525 °C. Using this optimal temperature (550 °C), they found that the efficiencies are improved thanks to suitable carrier concentration and mobility enhancement as well as an enlargement of grain size, which led to lower series resistance, higher fill factor and improved V_{oc}. As for pure Ge based kesterite CZGeSe, M. Buffière et al. [26] varied the annealing temperature from 460 °C to 500 °C using a one-step thermal profile for 15 min under H_2Se gas at atmospheric pressure. They selected, after an in-depth study, 460 °C as the most suitable temperature to obtain continuous and dense CZGeSe kesterite absorber layers, mentioning that large holes at the grain boundaries and voids at the Mo/CZGeSe interface appear when increasing temperature.

Regarding the present work, two approaches are presented to evaluate the best annealing conditions for pure Ge kesterite that ensure an optimal compromise crystallinity-efficiency. A comparison study is carried out between one- and two-step annealing profiles. The effect of temperature variation in each profile is also investigated. For the one-step process, the as-deposited precursors are annealed at three different temperatures (480 °C, 500 °C, and 525 °C) that are performed in selenium atmosphere at 1 bar working pressure for 10 min.

The effect of the temperature variation on the kesterite morphology is illustrated in Fig. 1. For the one-step annealing processes (top), it is discernible that the grain size increases slightly with increasing temperature, where the average grain size was about 665 nm for 480 °C annealing temperature and get moderately enlarged to 844 nm for 525 °C. In terms of crystalline quality, the FWHM of the main CZGeSe peak extracted from Raman spectra (Fig. 2) remains approximately intact (~10 cm^{-1}) for the three temperatures along with keeping the same peak position at 205 cm^{-1}.

As for the two-step annealing profile, the first annealing stage is set at 330 °C, whereas the second plateau is subjected to a temperature variation from 480 °C to 525 °C. Unlike what is found previously with the one-step temperature optimization, SEM images of the two-step selenization profile prove that small changes in temperature impact considerably the shape and size of the grains that became sharp with angular edges with elevated temperatures. Raman spectra ($\lambda_{excitation} = 442\,nm$)confirm this effect, through which the FWHM of the main CZGeSe peak (~205 cm^{-1}) knows a distinctly remarkable change and undergoes a systematic broadening from 9.1 cm^{-1} for 330 °C/480 °C to around 16 cm^{-1} for 330 °C/525 °C, alongside a small shift towards lower frequency of the order of 0.1 cm^{-1} (Fig. 2b inset) which prove that temperatures higher than 480 °C induce a degeneration of the kesterite crystalline quality that may be attributed to the formation of different defects at elevated temperatures and/or an increment in defect concentration detected on the absorber surface that according to Ray et al. [27] could be associated to an order-disorder transition of Cu–Zn atoms. Otherwise, X. Fontané et al. related this redshift to a slight lattice strain [28].

In the same manner, the peaks intensity of ZnSe secondary phase (~250 cm^{-1}) continued to increase with temperature until surpassing the principle peak of kesterite, indicating the decomposition of kesterite

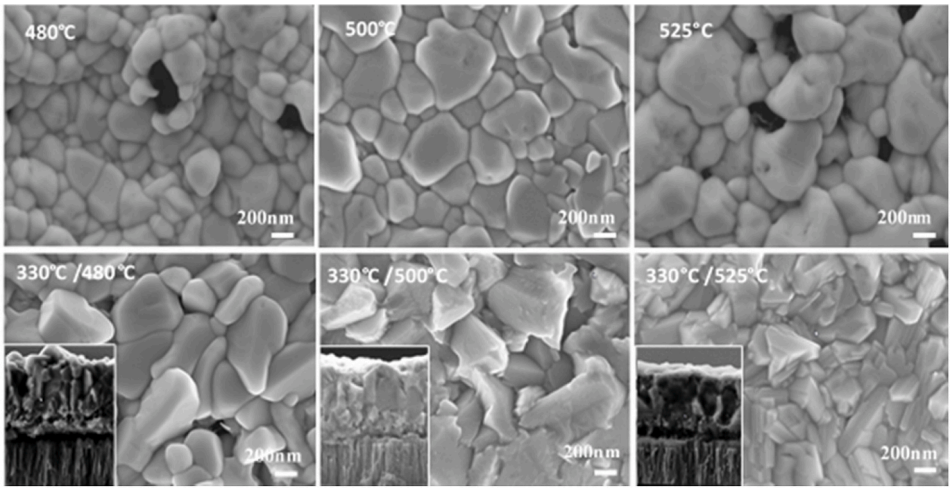

Fig. 1. SEM images of the effect of temperature variation on CZGeSe absorbers annealed with one-step annealing (top) and two-step annealing profiles with their respective cross-sections (bottom).

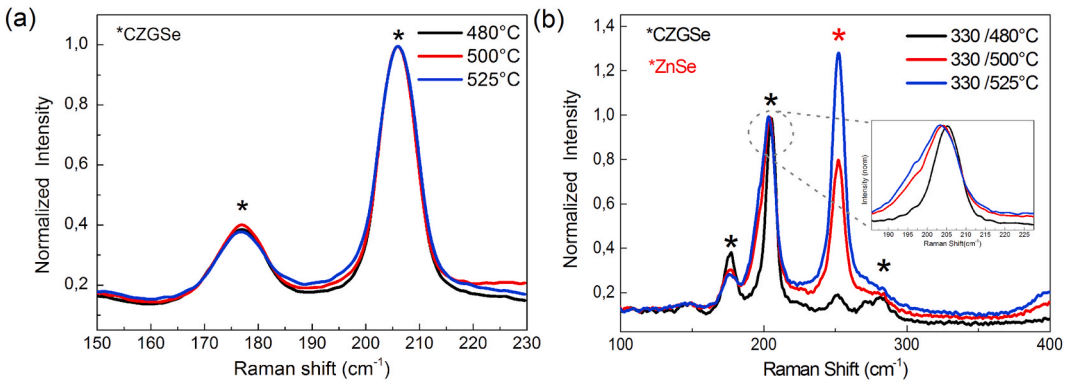

Fig. 2. Raman spectra of the effect of temperature variation on CZGeSe absorbers annealed with: (a) one-step annealing and (b) two-step annealing profiles.

into secondary phases.

It is worthy to note that the use of high temperatures in the second annealing step (330 °C/500–525 °C) creates severe inhomogeneities on the surface related to the presence of a massive amount of ZnSe secondary phase as shown in Fig. S1 which is in great accordance with the resulted Raman peak and is another indication of the detrimental effect of high temperatures on kesterite phase and the subsequent secondary phases formation.

Even though the absorber crystallinity remains unchanged during the temperature variation of the one-step annealing profile, the efficiency as all the electrical parameters witness a distinct change. As shown in Fig. 3, the electrical parameters are gradually improved as the annealing temperature is increased. Thus, the efficiency raises from 0.8% in the case of 480 °C to around 4% for 525 °C. With regards to the two-step profile as already mentioned, small variations in temperature higher than 330 °C/480 °C lead to the formation of large amounts of ZnSe secondary phase on the surface that hinders the conversion of these absorbers to solar cells (no photovoltaic effect). The best thermal treatment obtained from this optimization is the two-step annealing profile with low temperatures that gave higher performance devices compared to the best efficiency for the one-step annealing profile. The results of this study are summarized in Table 1, which shows the photovoltaic parameters of the best device for each annealing routine.

3.2. *Effect of surface treatment agent*

Even using optimal precursor composition and synthesis conditions, the thermodynamically stable kesterite single-phase remains a restrained region in the phase diagram [29]. Various secondary phases are prone to form during the absorber layer processing in the case of kesterite CZTSSe such as Zn(S,Se), $Cu_x(S,Se)$, $Sn(S,Se)_x$ or $Cu_2Sn(S,Se)_3$ [30]. The existence of these phases influences the resulting absorber quality tremendously due to their deleterious effect on band alignment, band gap fluctuations, carrier transport, increasing recombination rate,

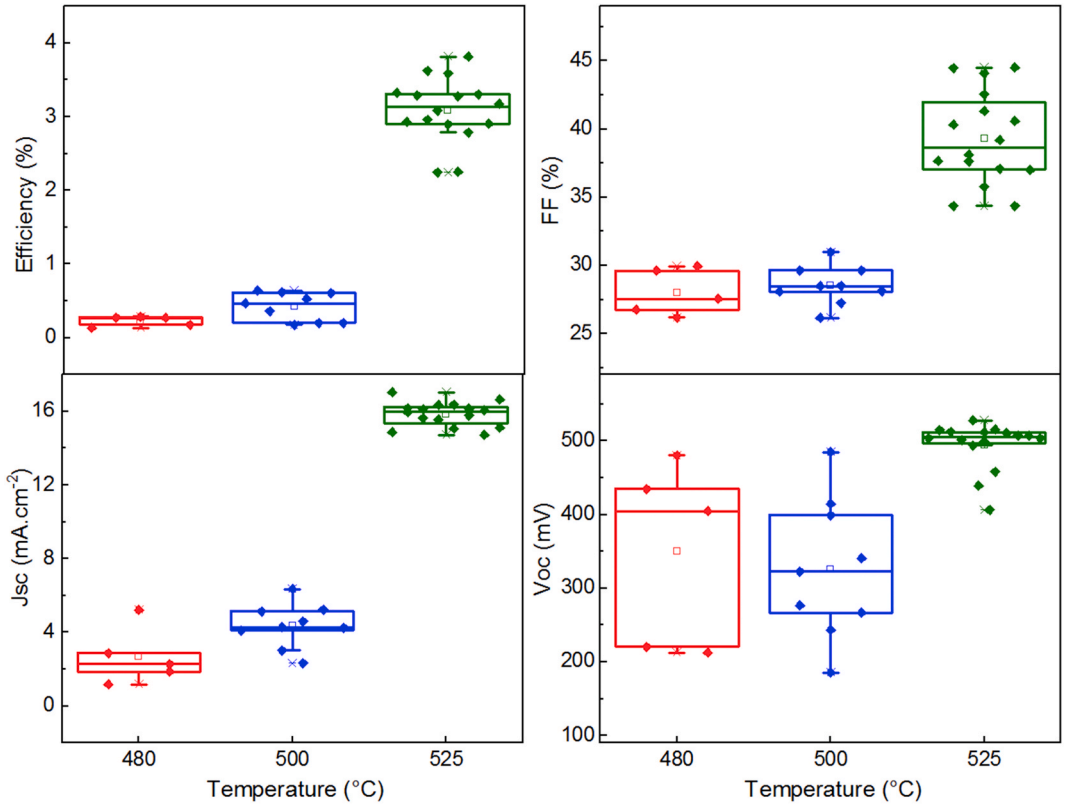

Fig. 3. Box chart representation of the temperature variation effect of one-step annealing process on the photovoltaic parameters.

Table 1
Photovoltaic parameters of the best devices fabricated using one- and two-step annealing profiles with different temperatures.

	One step annealing profile			Two-step annealing profile		
Temperature (°C)	480	500	525	330/480	330/500	330/525
Efficiency (%)	0.3	0.6	3.8	5.7	0	0
J_{sc} (mA/cm^2)	5.2	4.3	17.0	17.5	n/a	n/a
V_{oc} (mV)	212	484	503	572	n/a	n/a
FF (%)	26.0	31.0	44.5	65.0	n/a	n/a

n/a: not applicable (no PV effect is witnessed).

or on the mismatch in the crystal structure, among others [31]. Therefore, their removal constitutes a critical challenge for any further improvement in the kesterite-based solar cells performance. Choosing selective chemical etching agents that act on specific secondary phases has been a matter of concern for many research groups [32]. Several studies have shown that Zn related secondary phases mainly in the form of Zn(S,Se) stemmed from Zn-rich composition and tend to appear on the surface and/or at the back region of Se-rich CZTSSe absorbers [33]. Since avoiding this undesirable phase when present in the bulk and/or in the Mo/Absorber interface is unattainable, treating the absorber surface is the only remaining solution. For instance, $KMnO_4$ in acidic environments such as H_2SO_4 has indicated a great effectiveness in ZnSe removal by oxidizing Se^{2-} localized on the ZnSe phase surface [34]. On the other hand, and similarly to what was demonstrated for CIGS solar cells, KCN showed the same effect for kesterite-based solar cells by acting as a wet chemical remover of Cu–Se phases that are known to short circuit the diode [35]. Moreover, considering that Sn(S,Se) secondary phases appear in a less important content compared to Zn(S,Se) in kesterite absorbers, little attention has been given to its effect on the device performance. Nevertheless, H. Xie and co-workers [36] have reported on a new method for selectively removing the excess of Sn related undesirable phases. They concluded that $(NH_4)_2S$ yellow solution has demonstrated its success not only in Sn(S,Se) withdrawal but also by its ability to passivate the surface through the formation of S bonds from $(NH_4)_2S$ solution while removing oxygen bonds from the absorber surface. Aside from that, with this approach, the devices efficiency was increased from 4.6% to around 6% after etching.

To date, no clear evidence of useful surface etching treatments has been reported or implemented regarding CZGeSe absorber. Henceforth, an investigation in this sense has become a necessity. From this perspective, we report in the present work on a chemical wet etching study that intends to evaluate the effect of different etching agents on as annealed CZGeSe absorbers by immersing the samples in distinct solutions such as KCN, $(NH_4)_2S$ and $KMnO_4$+ $(NH_4)_2S$

The completed devices, using different absorbers treated with each etching agent, are characterized with AM1.5G solar simulator to extract their photovoltaic parameters (J-V curves are depicted in Fig. 4a). One can notice that V_{oc} made a huge leap from 368 mV for the unetched absorber, to 550 mV when the absorbers are treated in acidic environment with $KMnO_4$+ $(NH_4)_2S$, and increased further in the case of KCN etching to achieve values up to 580 mV. This is the highest V_{oc} obtained from this optimization. Whereas $(NH_4)_2S$ alone does not seem to improve the electrical parameters, contrariwise, it slightly lowers the V_{oc} compared to the unetched sample. This increment in V_{oc} drastically affects the corresponding efficiency that boosted from 3.7% without any etching to 5.7% in the case of KCN agent. Further details about the electrical parameters depending on the used etching agents are presented in Table 2.

The compositional ratios revealed by XRF remained unchanged after treating the surface of the absorber with the different etching agents. The ratios are balanced between 0.65 and 0.68 for Cu/(Ge + Zn) and in the range of 1–1.2 for Zn/Ge indicating a Zn rich composition, however, with Cu poorer conditions in comparison with the optimal ones commonly found in Sn-based kesterite [37]. This constancy in composition points out the limited effectiveness of the etching treatment on the secondary phase removal, which is confirmed by Raman spectra (not represented here), that demonstrated that no significant changes with the surface treatment regarding the ZnSe corresponding peak, since it is the likely expected secondary phase to appear in the case of CZGeSe as has been demonstrated elsewhere [38]. Hence, the hypothesis of improving the performance through the elimination of secondary phases using the studied agents is discarded. One possible route to explain the improved V_{oc} and FF is the passivation effect that occurs for the absorber surface associated with a reduction of non-radiative recombination states density and subsequent improvement of the p-n junction after the chemical treatment of the CZGeSe surface [34].

The EQE spectra depicted in Fig. 4b of the device etched with KCN show slightly higher EQE spectra response in the wavelength range of 600–800 nm, demonstrating an enhanced charge carrier collection and/or changes in the optical reflection of the surface, when compared to the unetched sample and the one etched with $(NH_4)_2S$. This indicates that the use of KCN slightly improves the interface quality by limiting the interface defects concentration within the diffusion length of the junction and reducing the trap assisted recombination, and/or affecting the optical properties of the CZGeSe/CdS interface. This behavior is in general in agreement with the improved device performance especially a boost in V_{oc} generally attributed to a surface passivation. The bandgap extracted from EQE does not seem to be affected by the etching agent, and is roughly estimated at 1.47 eV.

The V_{oc} deficit is another inescapable issue facing kesterite technology and may result either from the bulk material properties or from the superposed interfaces, and it is given by:

$$V_{oc}\ deficit = E_g/q - V_{oc}(exp) \quad (1)$$

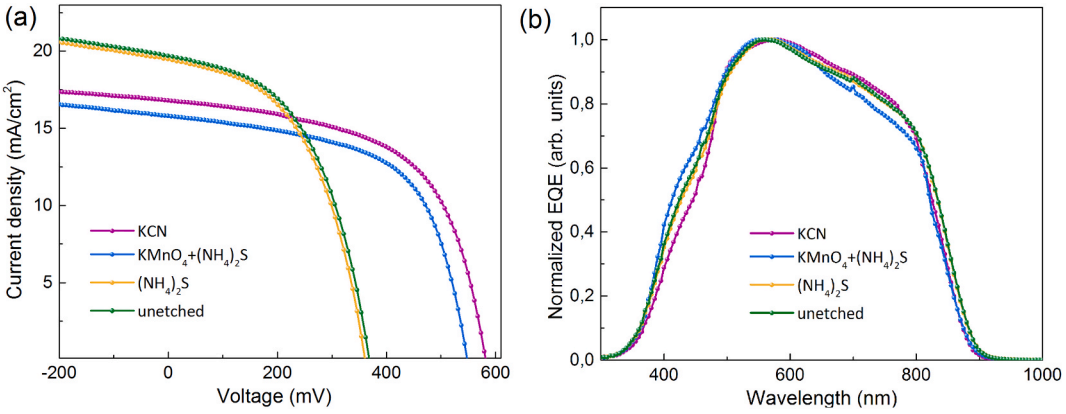

Fig. 4. J-V curves of CZGeSe subjected to different etching agents (a), and their corresponding normalized EQE spectra (b).

Table 2
Photovoltaic parameters and absorber composition for the unetched sample and the different surface-treated samples.

Etching Agent	Cu/(Ge + Zn)	Zn/Ge	J_{sc} (mA/cm^2)	V_{oc} (mV)	FF (%)	η(%)	V_{oc} deficit (mV)	SQ, V_{oc} deficit (mV)
unetched	0.68	1.15	19	368	50	3.7	1032	829
$(NH_4)_2S$	0.68	1.15	19	360	51	3.5	1040	837
$KMnO_4$+ $(NH_4)_2S$	0.66	1.12	16	548	59	5.2	852	649
KCN	0.67	1.06	17	582	58	5.7	818	615

$$SQ,\ V_{oc}deficit\ = V_{oc}(SQ\ limit) - V_{oc}(exp) \quad (2)$$

Where E_g is the absorber bandgap and q the elemental charge, V_{oc} (SQ limit) is the V_{oc} corresponding to the Shockley–Queisser limit and V_{oc}(exp) is experimentally measured under AM1.5G conditions.

The V_{oc} deficit witnesses a drop from 0.83 V for the unetched sample to 0.61 V for the sample etched with KCN with unchanged bandgap (~1.45 eV) as mentioned in Table 2. However, these values are still high compared to efficient CZTSSe and CZTGSe ones, found to be around 0.37 V and 0.35 V for a bandgap of 1.13 eV and 1.11 eV, respectively [39,40], which is expected to happen by widening the band gap [41].

To elucidate further the beneficial effect of KCN, we have estimated the Urbach energy (E_U) from EQE measurements in the region of the spectrum where the Urbach rule is satisfied (below E_g). Given that the band tails represent the disorder related to the width of the localized states available in the optical band gap and the defect states linked to impurities that cause voltage losses [42,43]. The plot presented in Fig. S2 shows a moderate mitigation of E_U from around 24 meV in the case of the unetched absorber to almost 22 meV for the sample etched with KCN. This could be tied to a passivation effect caused by a reduction of the density of recombination tail states below the bandgap, in addition to an improvement of the quality of the p-n junction leading to an increase in V_{oc} and FF, which is in good agreement with the prior optoelectrical observations. It is worthwhile to mention that the calculated E_U in this study is smaller than the one found for the same absorber synthesized by co-evaporation with a value of ~28 meV corresponding to E_g~1.4 eV [44]. E_U of about 33 meV was encountered within the best efficiency reported for CZTGSe material with E_g~1.31 eV [41]. These values stay far below the Sn kesterite case, estimated to be around 60 meV in the case of CZTSSe, and 70 meV for CZTS [45]. What has led to conclude that Ge atoms embedded in the kesterite lattice have a direct impact on Urbach energy reduction [46].

Lastly, combining the results of the optimal etching agent and the most favorable annealing profile and temperature acquired from this study, i.e. a two-step annealing at 330/480 °C followed by a wet chemical etching using KCN, we succeeded to obtain a solar cell device exhibiting an efficiency of 5.6% with a of V_{oc} = 572 mV, J_{sc} = 17.5 mA/cm^2 and FF = 65%. The AM1.5 illuminated J-V curve along with the EQE spectrum of the best CZGeSe solar cell are displayed in Fig. 5. The corresponding band gap is extracted from EQE and found to be around 1.5 eV.

3.3. Effect of post-annealing treatment on solar cells performance

As aforementioned, the V_{oc} limitation is the widespread and critical issue hampering performance improvements in kesterite-based solar cells. Research has tended to focus on recovering from this problem linked to the existence of recombination centers within the absorber, in the grain boundaries and/or at the interfaces, by performing a post low-temperature treatment (PLTT) [47,48]. Many studies have shed light on the positive impact of heat treatment (HT) on boosting the final yield of solar cells. Even if its effects are still not fully understood so far, its beneficial effect has been proven at different stages of the solar cell fabrication; by applying the temperature treatment on the as-annealed absorber, on the absorber/CdS junction, or on the complete solar cell (absorber/CdS/TCO) [49]. The heat treatment of CZTS/CdS interface has been conducted by many research groups, e.g., C. Yan et al. have found that the heterojunction annealing reduces the non-radiative recombination and favors the Na accumulation and out-diffusion from soda-lime glass (SLG) to the heterojunction that consequently induces a more favorable band alignment at the p-n interface. This has led to an improvement in the efficiency from 8% (without HT) to over 10% (at 270 °C for 10 min) [50]. In another study, H. Xie et al. showed the positive influence of the post-annealing on bare absorbers with a significant performance improvement, where they highlighted the importance of the Na distribution through the CZTSSe/CdS interface and its role in passivating defects in grain boundaries and at the interfaces [47]. By varying the temperature of HT from 150 °C to 400 °C, they noticed a performance deterioration at low temperatures but recovered again and overpassing remarkably the reference cell at 350–400 °C. They related this behavior to the considerable suppression of the high degree of tail states at high PLTT, which is directly linked to the distribution of Na in the solar cell and Cu–Na substitution. Otherwise, M. Neuschitzer et al. [51] proposed a comparison between the PLTT performed at different stages of CZTS solar cell fabrication and enlightened its strong impact on device performance, showing an efficiency increase from below 3% to up to 8.3% when applying a post-deposition annealing treatment on the complete cell at 200 °C for 35 min. Thus, they considered this latter as the optimal among all the HT performed on the other interfaces. Furthermore, they noticed changes in the surface composition,

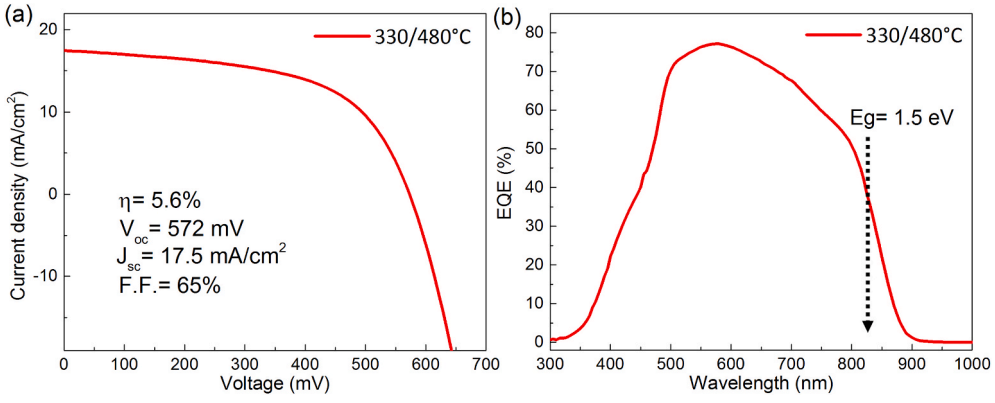

Fig. 5. J-V characteristics and EQE spectrum of the champion CZGeSe cell after etching and annealing optimizations.

becoming Cu poorer and Zn richer, which is the widely agreed consensus for achieving highly efficient devices. M.G. Sousa et al. [52] appear to support these findings and have shown that the most relevant boost in efficiency (from under 1% to over 6.6%) occurred when it is performed on finished solar cells and attributed this to some chemical modifications happening in the solar cell. They have assigned this effect to a Cu and Zn migration from the absorber to the CdS buffer layer and a Cd displacement in the opposite direction upon annealing.

To the best of our knowledge, no previous research has investigated before the post-annealing treatment in the case of CZGeSe based solar cells. For that purpose, our experiments intend to assess and unveil its effect on complete CZGeSe solar cells (stored for two months under vacuum conditions). As shown in Fig. 6a and detailed in Table S1, the performance of the stored cell has recovered from 4.4% to 5.4% accompanied by an increment in all electrical parameters after undergoing an annealing at 100 °C for 10 min in atmospheric pressure. The efficiencies stabilize again at around 4% for temperatures ranging from 150 °C to 300 °C, to drop completely at temperatures above 350 °C. J_{sc} and FF seem to follow a very similar trend, except the V_{oc} that remained stable and resisted until higher post-annealing temperatures.

These findings are in good agreement with the EQE spectra depicted in Fig. 6b that witnessed a continual decrease in the quantum efficiency from 75% in the reference sample (as-prepared solar cell) to barely efficiently working solar cells at higher post-annealing temperatures (350 °C–400 °C). The small quantum efficiency (QE) variation between 400 and 500 nm is generally attributed to loss mechanisms due to the light absorption in TCO and CdS layers that induce front recombination [53]. However, the major damage of the post-annealing is noticed above 550 nm, when the QE drops proportionally with increasing the temperature. The Urbach energy estimated from EQE increases gradually as function of hot plate soft annealing temperature, from 22 meV for the reference sample up to 34 meV for the sample post-annealed at 150 °C, and up to 38 meV for a post-annealing at 300 °C. This indicates a broadening of the band-tail region that can be originated from cation anti-site disordering and the subsequent electrostatic-potential fluctuation, due to the large amount of charged-defects in the absorber material. This proves that the state of ordering and disordering at the interface is strongly dependent on the post-annealing conditions, which in the case of CZGeSe increases linearly with temperature [22,54].

To get a deeper insight into the origin of these losses, taking into account that QE analysis affords an understanding of the photogenerated carrier collection in the device in addition to a spatial distribution of the dominant recombination path along the solar cell. Analytical descriptions have been designed to model bias-dependent quantum efficiency to study the behavior of CZTSe and CZTSe:Ge absorbers with different voltage and light bias conditions [55,56]. The QE response differs depending on the applied voltage bias (V_{bias}), where reverse bias seems not affecting the spectral response (optimized depletion width with improved carrier collection are conserved), whereas the forward bias (V_{bias} = 0.2 V) induces a strong decay in QE response at long-wavelengths more specifically. This behavior can be explained by the presence of deep ionized acceptor-type defects around the mid-gap, influencing the electric field and lead to an electronic doping by trapping holes from the valence band, which eventually lower the band bending of the CdS/CZTSSe interface layer and reduce the depletion width. Hence, inducing a strong decrease in the absorption in CZTSe. In other terms, the higher V_{bias}, the higher are the interface defects concentration, and the lower is the carrier collection efficiency which could be explained also by the presence of tail state recombination as previously indicated [57,58].

The “blue” light bias confirmed the presence of the interface defects near the heterojunction due to the compensation of the ionized defects impeding the carrier collection of the device. This light bias effect helped to extend the depletion layer and to increase the carrier collection of the absorber that consequently recover the QE response at long wavelengths (>550 nm).

As for the complete collapse of the EQE response above 300 °C, it could be attributed to the deterioration of CdS that not endures the post-annealing at high temperature and could form photoactive defects causing crossover and red-kink, therefore, degrading all the electrical metrics [59]. On the other hand, researches have proven that high post-annealing temperature induces an irreversible degradation in the CZTSe absorber through its decomposition in view of the migration of species such as the binary phase of Cu_xS, besides to Cu_{Zn} anti-site reordering transition occurring at elevated temperatures that engender the highest disorder level of Cu–Zn anti-site defects and give rise to inferior photovoltaic performance along with a notable increase in series resistance of CZTS solar cells [60,61]. Seemingly, the same phenomenon may occur with CZGeSe but for much lower temperatures.

The triangular shape of EQE stems from the strong carrier collection loss at the heterojunction interface, as explained earlier, and has been found even for the 12.6% champion device. The improvement of the diffusion length of minority carriers by improving the interface band offset, acting on less defective buffer represents the potential pathway to increase efficiency beyond the reported record [39,62].

In brief, this investigation has led us to conclude that the post-annealing treatment of complete CZGeSe solar cells does not lead to the same effects as in the case of Sn-based kesterite, but at the opposite, even the beneficial effect of alkalis diffusion (especially Na from SLG) widely encountered in CIGS and CZTS thin-films solar cells was not

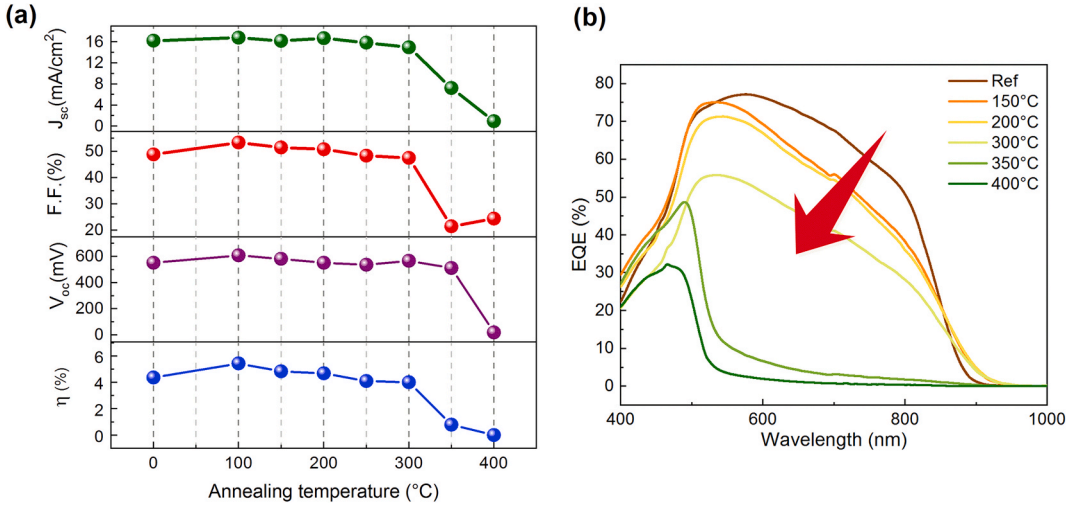

Fig. 6. Correlation of optoelectrical parameters as a function of HT temperature (a) and the corresponding EQE spectra(b).

noticed in our experiments on pure Ge kesterite [46]. However, the post-annealing treatment may help to recover to some extent the efficiency of these solar cells after long term storage, especially at lower temperatures (100 °C). Additional experiments are ongoing to shed more light on the effect of this post-annealing treatment.

4. Conclusions

This study has paved the way towards a better understanding of the annealing regime conditions and suitable surface treatments for $Cu_2ZnGeSe_4$ absorbers, since they are key parameters for the optimal synthesis of the semiconductor material, avoiding the presence of harmful secondary phases, and leading to high efficiency solar cells.

The experimental results demonstrate that the annealing conditions (i.e., thermal profile and temperature) have a direct impact on the absorber structural, morphological, and optoelectronic properties and small changes in temperature may induce a considerable effect on the absorber crystallinity, thus affecting the performance of the resulting solar cells.

In other respects, certain surface treatment agents used in this study, KCN in particular, have contributed to a drastic enhancement in CZGeSe solar cell performance. Interestingly, the overall compositional ratios remain almost intact in all etching cases tested. This leads to conclude that a possible surface passivation is responsible for this efficiency enhancement. Furthermore, KCN appears to act on the improvement of the p-n junction through a reduction of non-radiative recombination rather than removing secondary phases.

From these findings, the following conclusions are drawn:

1. The optimal crystallinity and material properties of $Cu_2ZnGeSe_4$ is achievable at low annealing temperatures leading to the same grain size encountered in Sn-based kesterite at higher temperatures. The lower synthesis temperatures result in a clear advantage compared to other kesterite systems, especially interesting for monolithic integration in tandem solar cell concepts.
2. The two-step annealing profile using lower temperatures compared to one-step processes is considered as the most suited regime that produced a significant performance improvement (from 3.8% to 5.7%).
3. Using the higher annealing temperatures when adopting the two-step annealing regime creates inhomogeneities on the absorber surface caused by huge amounts of ZnSe on the surface, which impeded the fabrication of working solar cells. High temperatures led to degraded grains morphology.
4. By treating the absorber surface with KCN, the V_{oc} is boosted from 370 mV to 580 mV maintaining the same bandgap (~1.4 eV), leading to a V_{oc} deficit reduction from 1.1 V to 0.8 V. Similar results were obtained with a combination of $KMnO_4$+ $(NH_4)_2S$, being an interesting route to further optimize in the future to avoid the use of highly toxic chemicals like KCN.
5. CZGeSe synthesized in this study with the optimal conditions demonstrated a very low Urbach energy of about 22 meV for the best performing devices, which shows remarkably improved values compared to Sn-based kesterite.
6. Unlike what has been found in the case of CZT(S,Se), the post-annealing treatment of completed solar cells (Mo/CZGeSe/CdS/i-ZnO/ITO) has been proven ineffective for enhancing the overall performance, but it has rather shown a detrimental effect on the overall photovoltaic parameters with increasing post-annealing treatment temperatures, especially over 300 °C.

Declaration of competing interest

The authors declare that they have no known competing financial interests or personal relationships that could have appeared to influence the work reported in this paper.

CRediT authorship contribution statement

Nada Benhaddou: Writing - original draft, performed the experiments and the devices fabrication and characterization, as well as the discussion of the results and wrote the manuscript. **Safae Aazou:** Writing - original draft, Supervision, supervised the work and helped in the discussion and interpretation of the results besides, she contributed in the writing of the paper and revised the manuscript, with contributions from all authors. **Yudania Sánchez:** performed the buffer/window layer deposition for the devices fabrication and contributed to the electrical characterization of the solar cells. **Jacob Andrade-Arvizu:** contributed in the absorber synthesis and the discussion of the results. **Ignacio Becerril-Romero:** Formal analysis, carried out the compositional analysis characterization along with the analysis of the results. **Maxim Guc:** Formal analysis, performed the Raman measurements, analyzed and discussed the results. **Sergio Giraldo:** Formal analysis, performed the SEM characterization and participated in the discussion and data analysis. **Victor Izquierdo-Roca:** helped with the Raman results interpretation and their discussion. **Edgardo Saucedo:** Supervision, and. **Zouheir Sekkat:** Supervision, conceived the idea, participated in the discussion of the results and supervised the work.

Acknowledgments

We gratefully acknowledge the help provided by INFINITE CELL project (H2020-MSCA-RISE-2017 777968), by the Spanish Ministry of Science, Innovation, and Universities under the IGNITE (ENE2017-87671-C3-1-R), by the European Regional Development Funds (ERDF, FEDER Programa Competitivitat de Catalunya 2007–2013) and CERCA Programme/Generalitat de Catalunya. and the help carried out by the project PPR/2015/59 funded by the Moroccan Ministry of Higher Education and Research. Authors from IREC belong to the SEMS (Solar Energy Materials and Systems) Consolidated Research Group of the "Generalitat de Catalunya" (Ref. 2017 SGR 862).

Appendix A. Supplementary data

Supplementary data to this article can be found online at https://doi.org/10.1016/j.solmat.2020.110701.

References

[1] Y. Zhang, R.E. Bartolo, S.J. Kwon, M. Dagenais, High short-circuit current density in CIS solar cells by a simple two-step selenization process with a KF postdeposition treatment, IEEE J. Photovoltaics 7 (2) (2017) 676–683, https://doi.org/10.1109/JPHOTOV.2016.2636999.
[2] C.H. Wu, P.W. Wu, J.H. Chen, J.Y. Kao, C.Y. Hsu, Effect of selenization processes on CIGS solar cell performance, J. Nanosci. Nanotechnol. 18 (7) (2018) 5074–5081, https://doi.org/10.1166/jnn.2018.15279.
[3] L. Zhang, D. Zhuang, M. Zhao, Q. Gong, L. Guo, L. Ouyang, R. Sun, Y. Wei, S. Zhan, The effects of annealing temperature on CIGS solar cells by sputtering from quaternary target with Se-free post annealing, J. Appl. Surf. Sci. 413 (15) (2017) 175–180, https://doi.org/10.1016/j.apsusc.2017.03.289.
[4] T.R. Bai, C.Q. Liu, N. Wang, S.M. Liu, H.L. Wang, W.W. Jiang, W.Y. Ding, W.D. Fei, W.P. Chai, Effects of sputtering voltage and current on the composition and microstructureof the CIGS films prepared by one-step pulsed DC magnetron sputtering, J. Alloys Compd. (2015), https://doi.org/10.1016/j.jallcom.2015.06.077.
[5] W.-T. Lin, S.-H. Chen, S.-H. Chan, S.-C. Hu, W.-X. Peng, Y.-T. Lu, Crystallization phase transition in the precursors of CIGS films by Ar-ion plasma etching process, Vacuum 99 (2014) 1–6, https://doi.org/10.1016/j.vacuum.2013.04.012.
[6] A. Kanevce, M.O. Reese, T.M. Barnes, S.A. Jensen, W.K. Metzger, The roles of carrier concentration and interface, bulk, and grain-boundary recombination for 25% efficient CdTe solar cells, J. Appl. Phys. 121 (2017) 214506, https://doi.org/10.1063/1.4984320.
[7] A. Romeo, D.L. Bätzner, H. Zogg, A.N. Tiwari, Recrystallization in CdTe/CdS, Thin Solid Films 361–362 (21) (2000) 420–425, https://doi.org/10.1016/S0040-6090(99)00753-1.
[8] M. Kim, S. Sohn, S. Lee, Reaction kinetics study of CdTe thin films during CdCl2 heat treatment, Sol. Energy Mater. Sol. Cell. 95 (2011) 2295–2301, https://doi.org/10.1016/j.solmat.2011.03.044.
[9] I.M. Dharmadasa, P.A. Bingham, O.K. Echendu, H.I. Salim, T. Druffel, R. Dharmadasa, G.U. Sumanasekera, R.R. Dharmasena, M.B. Dergacheva, K.A. Mit,

K.A. Urazov, L. Bowen, M. Walls, A. Abbas, Fabrication of CdS/CdTe-based thin film solar cells using an electrochemical technique, Coatings 4 (3) (2014) 380–415, https://doi.org/10.3390/coatings4030380.
[10] S. Girish Kumar, K.S.R. Koteswara Rao, Physics and chemistry of CdTe/CdS thin film heterojunction photovoltaic devices: fundamental and critical aspects, Energy Environ. Sci. 1 (7) (2014) 45–102, https://doi.org/10.1039/C3EE41981A.
[11] Suneth C. Watthage, Geethika K. Liyanage, Zhaoning Song, Fadhil K. Alfadhili, Rabee B. Alkhayat, Khagendra P. Bhandari, Randy J. Ellingson, Adam B. Phillips, Michael J. Heben, Novel, facile back surface treatment for CdTe solar cells, in: IEEE 44th Photovoltaic Specialist Conference (PVSC), Washington, DC, 2017, pp. 815–819, https://doi.org/10.1109/PVSC.2017.8366216.
[12] T.-P. Hsieh, C.-C. Chuang, C.-S. Wu, J.-C. Chang, J.-W. Guo, W.-C. Chen, Effects of residual copper selenide on cuingase2 solar cells, Solid State Electron. 56 (1) (2011) 175–178, https://doi.org/10.1016/j.sse.2010.11.019.
[13] J. Jiang, R. Giridharagopal, E. Jedlicka, K. Sun, S. Yu, S. Wu, Y. Gong, W. Yan, D. S. Ginger, M.A. Green, X. Hao, W. Huang, H. Xin, Highly efficient copper-rich chalcopyrite solar cells from DMF molecular solution, Nano Energy (2020), https://doi.org/10.1016/j.nanoen.2019.104438.
[14] J. Li, Y. Ma, G. Chen, J. Gong, X. Wang, Y. Kong, X. Ma, K. Wang, W. Li, C. Yang, X. Xiao, Effects of ammonia-induced surface modification of Cu(In,Ga)Se_2 on high-efficiency Zn(O,S)-Based Cu(In,Ga)Se_2 solar cells, RRL Solar 3 (21) (2019) 800254, https://doi.org/10.1002/solr.201800254.
[15] E. Garcia-Llamas, J.M. Merino, R. Gunder, K. Neldner, D. Greiner, A. Steigert, S. Giraldo, V. Izquierdo-Roca, E. Saucedo, M. León, S. Schorr, R. Caballero, Cu_2ZnSnS_4 thin film solar cells grown by fast thermal evaporation and thermal treatment, Sol. Energy 141 (2016) 236–241, https://doi.org/10.1016/j.solener.2016.11.035.
[16] D.B. Mitzi, O. Gunawan, T.K. Todorov, K. Wang, S. Guha, The path towards a high-performance solution-processed kesterite solar cell, Sol. Energy Mater. Sol. Cells 95 (6) (2011) 1421–1436, https://doi.org/10.1016/j.solmat.2010.11.028.
[17] D. Pareek, T. Taskesen, J.A. Márquez, H. Stange, S. Levcenco, I. Simsek, D. Nowak, T. Pfeiffelmann, W. Chen, C. Stroth, M.H. Sayed, U. Mikolajczak, J. Parisi, T. Unold, R. Mainz, L. Gütay, Reaction pathway for efficient Cu2ZnSnSe4 solar cells from alloyed Cu-Sn Precursor via a Cu-Rich selenization stage. https://doi.org/10.1002/solr.202000124, 2020.
[18] S. Kim, J. Park, A. Walsh, Identification of killer defects in kesterite. https://doi.org/10.1021/acsenergylett.7b01313, 2018.
[19] X. Liu, Y. Feng, H. Cui, F. Liu, X. Hao, G. Conibeer, D.B. Mitzi, M. Green, The current status and future prospects of kesterite solar cells : a brief review, Progress Photovolt. (2016) 879–898, https://doi.org/10.1002/pip.2741. January.
[20] P. Jackson, R. Wuerz, D. Hariskos, E. Lotter, W. Witte, M. Powalla, Effects of heavy alkali elements in Cu(In , Ga)Se2 solar cells with efficiencies up to 22.6 %, Phys. Status Solidi (RRL) - Rapid Res. Lett. 586 (8) (2016) 583–586, https://doi.org/10.1002/pssr.201600199.
[21] S. Sahayaraja, G. Brammertza, B. Vermang, T. Schnabel, E. Ahlswede, Z. Huang, S. Ranjbar, M. Meurisa, J. Vleugels, J. Poortmans, Optoelectronic properties of thin film $Cu_2ZnGeSe_4$ solar cells, Sol. Energy Mater. Sol. Cell. 171 (May) (2017) 136–141, https://doi.org/10.1016/j.solmat.2017.06.050.
[22] J. Li, D. Wang, X. Li, Y. Zeng, Y. Zhang, Cation substitution in earth-abundant kesterite photovoltaic materials, Adv. Sci. 5 (4) (2018), https://doi.org/10.1002/advs.201700744.
[23] S. Kumar, D.K. Sharma, B. Joshi, S. Auluck, Theoretical insights into kesterite and stannite phases of $Cu_2(Sn_{1-X}\ Ge_X)\ ZnSe_4$ based alloys: a prospective photovoltaic material, AIP Adv. 6 (12) (2016), https://doi.org/10.1063/1.4971323.
[24] A. Fairbrother, X. Fontané, V. Izquierdo-Roca, M. Placidi, D. Sylla, M. Espindola-Rodriguez, S. López-Mariño, F.A. Pulgarín, O. Vigil-Galán, A. Pérez-Rodríguez, E. Saucedo, Secondary Phase Formation in Zn-Rich $Cu_2ZnSnSe_4$ - Based Solar Cells Annealed in Low Pressure and Temperature Conditions, 2014, pp. 479–487, https://doi.org/10.1002/pip.2473. January.
[25] A.C. Lokhande, R.B.V. Chalapathy, J.S. Jang, P.T. Babar, M.G. Gang, C. D. Lokhande, Jin Hyeok Kim, Fabrication of pulsed laser deposited Ge doped CZTSSe thin film based solar cells: influence of selenization treatment, Sol. Energy Mater. Sol. Cells 161 (September 2016) (2017) 355–367, https://doi.org/10.1016/j.solmat.2016.12.016.
[26] M. Meuris, J. Poortmans, Physical characterization of $Cu_2ZnGeSe_4$ thin films from annealing of Cu-Zn-Ge precursor layers, Thin Solid Films (2014), https://doi.org/10.1016/j.tsf.2014.09.024.
[27] G. Rey, A. Redinger, J. Sendler, T.P. Weiss, M. Thevenin, M. Guennou, B. El Adib, S. Siebentritt, The band gap of $Cu_2ZnSnSe_4$: effect of order-disorder, Appl. Phys. Lett. 105 (2014) 112106, https://doi.org/10.1063/1.4896315.
[28] X. Fontané, L. Calvo-Barrio, V. Izquierdo-Roca, E. Saucedo, A. Pérez-Rodriguez, J. R. Morante, D.M. Berg, P.J. Dale, S. Siebentritt, In-depth resolved Raman scattering analysis for the identification of secondary phases: characterization of Cu_2ZnSnS_4 layers for solar cell applications", Appl. Phys. Lett. 98 (2011) 181905, https://doi.org/10.1063/1.3587614.
[29] S. Chen, X.G. Gong, A. Walsh, S. Wei, Crystal and electronic band structure of Cu_2 $ZnSnX_4$,, X = S and Se … photovoltaic absorbers: first-principles insights, Appl. Phys. Lett. 94 (2009) 25–27, https://doi.org/10.1063/1.3074499, 041903.
[30] M. Buffiere, G. Brammertz, S. Sahayaraj, M. Batuk, S. Khelifi, D. Mangin, A. El Mel, L. Arzel, J. Hadermann, M. Meuris, J. Poortmans, KCN chemical etch for interface engineering in $Cu_2ZnSnSe_4$ solar cells, ACS Appl. Mater. Interfaces 7 (2015) 27, https://doi.org/10.1021/acsami.5b02122.
[31] W. Bao, M. Ichimura, Influence of secondary phases in kesterite-Cu_2ZnSnS_4 absorber material based on the first principles calculation, Int. J. Photoenergy 2015 (2015), https://doi.org/10.1155/2015/592079.
[32] A. Fairbrother, E. Garc, V. Izquierdo-roca, X. Fontane, Development of a selective chemical etch to improve the conversion efficiency of Zn-rich Cu_2ZnSnS_4 solar cells, J. Am. Chem. Soc. 134 (19) (2012) 8018–8021, https://doi.org/10.1021/ja301373e, 1–4.
[33] H. Xie, M. Dimitrievska, X. Fontané, Y. Sánchez, S. López-Marino, V. Izquierdo-Roca, V. Bermúdez, A. Pérez-Rodríguez, E. Saucedo, Formation and impact of secondary phases in Cu-poor Zn-rich Cu2ZnSn ($S_{1-y}\ Se_y$) 4 ($0 \leq y \leq 1$) based solar cells, Sol. Energy Mater. Sol. Cells 140 (2015) 289–298, https://doi.org/10.1016/j.solmat.2015.04.023.
[34] S. Lpez-Marino, Y. Snchez, M. Placidi, A. Fairbrother, M. Espindola-Rodriguez, X. Fontane, V. Izquierdo-Roca, Juan Lpez-Garcia, L. Calvo-Barrio, A. Perez-Rodriguez, E. Saucedo, ZnSe etching of Zn-rich $Cu_2ZnSnSe_4$: an oxidation route for improved solar-cell efficiency, Chem. Eur J. 19 (44) (2013) 14814–14822, https://doi.org/10.1002/chem.201302589.
[35] S. Niki, P.J. Fons, A. Yamada, Y. Lacroix, H. Shibata, H. Oyanagi, M. Nishitani, T. Negami, T. Wada, Effects of the surface $Cu_{2-x}Se$ phase on the growth and properties of $CuInSe_2$ films, Appl. Phys. Lett. 74 (11) (1999) 1630–1632, https://doi.org/10.1063/1.123639.
[36] M. Neuschitzer, D. Sylla, A. Fairbrother, V. Izquierdo-roca, A. Pe, E. Saucedo, Impact of Sn(S,Se) secondary phases in $Cu_2ZnSn(S,Se)_4$ solar cells: a chemical route for their selective removal and absorber surface passivation. https://doi.org/10.1021/am502609c, 2014.
[37] S. Chen, A. Walsh, X. Gong, S. Wei, Classification of lattice defects in the kesterite Cu2ZnSnS4 and Cu2ZnSnSe4 earth-abundant solar cell absorbers, Adv. Mater. (2013) 1–18, https://doi.org/10.1002/adma.201203146.
[38] N. Benhaddou, S. Aazou, R. Fonoll-Rubio, c Y. Sanchez, S. Giraldo, M. Guc, L. Calvo Barrio, V. Izquierdo Roca, M. Abd-Lefdil, Z. Sekkat, E. Saucedo, Uncovering details behind the formation mechanisms of $Cu_2ZnGeSe_4$ photovoltaic absorbers, J. Mater. Chem. C (2020), https://doi.org/10.1039/C9TC06728K.
[39] W. Wang, M.T. Winkler, O. Gunawan, T. Gokmen, T.K. Todorov, Y. Zhu, D.B. Mitzi, Device characteristics of CZTSSe thin-film solar cells with 12.6% efficiency, Adv. Energy Mater. (2013) 1–5, https://doi.org/10.1002/aenm.201301465.
[40] S. Kim, K.M. Kim, H. Tampo, H. Shibata, S. Niki, Improvement of voltage deficit of Ge-incorporated kesterite solar cell with 12.3% conversion efficiency, Appl. Phys. Expr. (1882) 1–5, https://doi.org/10.7567/APEX.9.102301, 2016.
[41] T. Schnabel, M. Seboui, E. Ahlswede, Band gap tuning of $Cu_2ZnGeS_xSe_{4-x}$ absorbers for thin-film solar cells, Energies 10 (11) (2017) 1813, https://doi.org/10.3390/en10111813, 2017.
[42] S. Zaynobidinov, R.G. Ikramov, R.M. Jalalov, Urbach energy and the tails of the density, J. Appl. Spectrosc. 78 (2) (2011) 243–247, https://doi.org/10.1007/s10812-011-9450-9.
[43] G. Reya, G. Larramona, S. Bourdais, C. Choné, B. Delatouche, A. Jacob, G. Dennler, S. Siebentritt, On the origin of band-tails in kesterite, Sol. Energy Mater. Sol. Cells (October) (2017) 1–10, https://doi.org/10.1016/j.solmat.2017.11.005.
[44] E. Ojeda-durán, K. Mon, J. Andrade-arvizu, I. Becerril-romero, Y. Sánchez, CZTS solar cells and the possibility of increasing V_{OC} using evaporated Al_2O_3 at the CZTS/CdS interface, Solar Energy 198 (January) (2020) 696–703, https://doi.org/10.1016/j.solener.2020.02.009.
[45] K. Nagaya, S. Fujimoto, H. Tampo, S. Kim, M. Nishiwaki, Y. Nishigaki, Very small tail state formation in $Cu_2ZnGeSe_4$, Appl. Phys. Lett. 113 (2018), 093901, https://doi.org/10.1063/1.5031799.
[46] H. Xie, S. Lopez-Marino, T. Olar, Y. Sánchez González, M. Neuschitzer, F. Oliva, S. Giraldo, V. IzquierdoRoca, I. Lauermann, A. Pérez-Rodríguez, E. Saucedo, Impact of Na dynamics at the $Cu_2ZnSn(S,Se)_4$/CdS interface during post low temperature treatment of absorbers, ACS Appl. Mater. Interfaces 8 (7) (2016) 5017–5024, https://doi.org/10.1021/acsami.5b12243.
[47] G. Rey, T.P. Weiss, J. Sendler, A. Finger, C. Spindler, F. Werner, M. Melchiorre, M. Hála, M. Guennou, S. Siebentritt, Ordering kesterite improves solar cells: a low temperature post-deposition annealing study, Sol. Energy Mater. Sol. Cell. 151 (2016) 131–138, https://doi.org/10.1016/j.solmat.2016.02.014.
[48] D. Hironiwaa, N. Sakai, T. Katob, H. Sugimotob, Z. Tang, J. Chantana, T. Minemoto, Impact of annealing treatment before buffer layer deposition on $Cu_2ZnSn(S,Se)_4$ solar cells, Thin Solid Films 582 (2014) 151–153, https://doi.org/10.1016/j.tsf.2014.11.016.
[49] C.R. Osterwald, T.J. McMahon, History of accelerated and qualification testing, Prog. Photovolt. Res. Appl. 17 (October 2016) (2009) 11–33, https://doi.org/10.1002/pip.861.
[50] C. Yan, J. Huang, K. Sun, S. Johnston, Y. Zhang, H. Sun, A. Pu, M. He, F. Liu, K. Eder, L. Yang, J.M. Cairney, N.J. Ekins-Daukes, Z. Hameiri, J.A. Stride, S. Chen, M.A. Green, X. Hao, Cu_2ZnSnS_4 solar cells with over 10% power conversion efficiency enabled by heterojunction heat treatment, Nat. Energy 3 (9) (2018) 764–772, https://doi.org/10.1038/s41560-018-0206-0.
[51] M. Neuschitzer, Y. Sanchez, T. Olar, T. Thersleff, S. Lopez, The complex surface chemistry of kesterites : Cu/Zn re-ordering after low temperature post deposition annealing and its role in high performance devices, Chem. Mater. (2015) 1–11, https://doi.org/10.1021/acs.chemmater.5b01473.
[52] M.G. Sousa, A.F. da Cunha, J.P. Teixeira, J.P. Leitão, G. Otero-Irurueta, M.K. Singh, Optimization of post-deposition annealing in Cu_2ZnSnS_4 thin film solar cells and its impact on device performance, Sol. Energy Mater. Sol. Cells 170 (March) (2017) 287–294, https://doi.org/10.1016/j.solmat.2017.05.065.
[53] A. Nakane, H. Tampo, M. Tamakoshi, S. Fujimoto, K.M. Kim, S. Kim, H. Shibata, S. Niki, H. Fujiwara, Quantitative determination of optical and recombination losses in thin-film photovoltaic devices based on external quantum efficiency analysis, J. Appl. Phys. 120 (2016), 064505, https://doi.org/10.1063/1.4960698.
[54] M.M. Islam, M.A. Halim, T. Sakurai, N. Sakai, T. Kato, H. Sugimoto, H. Tampo, H. Shibata, S. Niki, K. Akimoto, Determination of deep-level defects in Cu2ZnSn(S,

Se)4 thin-films using photocapacitance method, J. Appl. Phys. Lett. 106 (2015) 243905, https://doi.org/10.1063/1.4922810.
[55] S. Lee, K. Price, Spectral responses in quantum efficiency of emerging kesterite thin-film solar cells, Optoelectron. - Adv. Device Struct. (2017), https://doi.org/10.5772/68058.
[56] S. Lee, K.J. Price E. Saucedo, S. Giraldo, Improved quantum efficiency models of CZTSe: Ge nanolayer solar cells with a linear electric field, Nanoscale 10 (2018) 2990–2997, https://doi.org/10.1039/C7NR08824H.
[57] S. Lee, K.J. Price, Variation of quantum efficiency in CZTSSe solar cells with temperature and bias dependence by SCAPS simulation, J. Energy Power Eng. 11 (2017) 69–77, https://doi.org/10.17265/1934-8975/2017.02.001.
[58] C.J. Hages, N.J. Carter, R. Agrawal, Generalized quantum efficiency analysis for non-ideal solar cells: case of $Cu_2ZnSnSe_4$, J. Appl. Phys. 119 (2016), 014505, https://doi.org/10.1063/1.4939487.
[59] S. Tajima, M. Umehara, M. Hasegawa, T. Mise, T. Itoh, Cu_2ZnSnS_4 photovoltaic cell with improved efficiency fabricated by high-temperature annealing after CdS buffer-layer deposition, Prog. Photovoltaics Res. Appl. 25 (2017) 14–22, https://doi.org/10.1002/pip.2837.
[60] R. Chen, J. Fan, C. Liu, X. Zhang, Y. Shen, Y. Mai, Solution-Processed one-dimensional ZnO@CdS heterojunction toward efficient Cu_2ZnSnS_4 solar cell with inverted structure, Sci. Rep. 6 (2016), https://doi.org/10.1038/srep35300. Article number: 35300.
[61] S. Zhang, N.D. Pham, T. Tesfamichael, J. Bell, H. Wang, Thermal effect on CZTS solar cells in different process of ZnO/ITO window layer fabrication, Sustain. Mater. Technol. 18 (2018), e00078, https://doi.org/10.1016/j.susmat.2018.e00078.
[62] S. N Hood, A. Walsh, C. Persson, K. Iordanidou, D. Huang, M. Kumar, Z. Jehl, M. Courel, J. Lauwaert, S. Lee, Status of materials and device modelling for kesterite solar cells, J. Phys.: Energy 1 (4) (2019) 20, https://doi.org/10.1088/2515-7655/ab2dda.